Published in final edited form as:
Phys Rev E Stat Nonlin Soft Matter Phys. 2014 November ; 90(0): 053014.

Two-dimensional simulation of red blood cell motion near a wall under a lateral force

Daniel S. Hariprasad[1,*] and **Timothy W. Secomb**[2]

[1]Program in Applied Mathematics, University of Arizona, Tucson, AZ, 85721, USA

[2]Department of Physiology, University of Arizona, Tucson, AZ, 85724, USA

Abstract

The motion of a red blood cell suspended in a linear shear flow adjacent to a fixed boundary subject to an applied lateral force directed towards the boundary is simulated. A two-dimensional model is used that represents the viscous and elastic properties of normal red blood cells. Shear rates in the range of 100 s^{-1} to 600 s^{-1} are considered, and the suspending medium viscosity is 1 cP. In the absence of a lateral force, the cell executes a tumbling motion. With increasing lateral force, a transition from tumbling to tank-treading is predicted. The minimum force required to ensure tank-treading increases non-linearly with the shear rate. Transient swinging motions occur when the force is slightly larger than the transition value. The applied lateral force is balanced by a hydrodynamic lift force resulting from the positive orientation of the long axis of the cell with respect to the wall. In the case of cyclic tumbling motions, the orientation angle takes positive values through most of the cycle, resulting in lift generation. These results are used to predict the motion of a cell close to the outer edge of the cell-rich core region that is generated when blood flows in a narrow tube. In this case, the lateral force is generated by shear-induced dispersion, resulting from cell-cell interactions in a region with a concentration gradient. This force is estimated using previous data on shear-induced dispersion. The cell is predicted to execute tank-treading motions at normal physiological hematocrit levels, with the possibility of tumbling at lower hematocrit levels.

I. INTRODUCTION

An important consequence of the non-continuum behavior of blood flowing in microvessels is the formation of a cell-free layer near the vessel wall. A single red blood cell placed near a solid boundary in shear or Poiseuille flow migrates away from the wall as a consequence of fluid dynamic cell-wall interactions. This migration depends on the cell's deformability and does not occur for rigid particles, as such migration would be inconsistent with the reversibility of Stokes flow. Experimentally, a cell-free (or cell-depleted) layer is observed at the wall when blood flows through glass tubes or living microvessels. As a result, the apparent viscosity of blood in narrow tubes can be lower than the bulk viscosity, a phenomenon termed the Fahraeus-Lindqvist effect [1]. By comparing experimentally measured apparent viscosities in glass tubes with diameters in the range 30 to 1000 μm with

*dshari@math.arizona.edu.

predictions of a simple two-phase theory, Secomb [2] estimated that this layer has an effective width of 1.8 μm in such tubes.

Blood is a concentrated suspension of red blood cells, and cell-cell interactions also influence the lateral migration of an individual cell. The multiple interactions between suspended particles that occur in shear flow generally lead to net migration across the flow and down the gradient in particle concentration, an effect known as shear-induced dispersion or shear-induced diffusion [3, 4]. This effect drives red blood cells away from the region of higher concentration in the central core of the flow and counteracts the tendency of individual particles to migrate away from the walls, as indicated schematically in Figure 1 (a). It is reasonable to hypothesize that the width of the cell-free layer is determined primarily by the competing effects of cell-wall and cell-cell interactions [5].

Detailed numerical simulations of the motion of multiple red blood cells in cylindrical tubes by Fedosov et al. [6] have provided predictions of the cell-free layer width that agree well with the estimate stated above, and have also predicted apparent viscosity as a function of diameter in good agreement with experimental data obtained using glass tubes [7]. Such simulations support the hypothesis that fluid dynamic interactions determine the cell-free layer width. This approach requires numerically intensive computations for each case of interest. Also, the complexity of the simulations makes it difficult to deduce fundamental mechanisms underlying the behavior that is being simulated.

Pranay et al. [8] considered the balance between shear-induced migration towards the wall and migration away from the wall resulting from cell-wall interactions. In their theory, the cell-wall interaction is estimated assuming a dipole approximation for the flow perturbation induced by the particle. While this is appropriate for cells that are relatively far from the wall (compared to cell size), it does not provide a good approximation for cells close to the wall. Since the typical cell-free layer width at physiological hematocrit, about 2 μm, is small relative to the diameter of a red cell, about 8 μm, a theory that is applicable for close interactions between the cell and the wall is desirable.

Grandchamp et al. [9] experimentally examined the lift generated by a red blood cell near a wall in shear flow and shear-induced dispersion in a suspension of red blood cells. Their results showed that red blood cells tumbling near a wall in shear flow generate a lift and migrate away from the wall. However, they did not clearly identify how a tumbling red blood cell generates lift, whereas a tumbling rigid particle does not. In a separate experiment, they examined the shear-induced dispersion of a cloud of red blood cells and estimated the dispersion coefficient.

In this paper, we develop a model for the motion of a red blood cell in a shear flow over a solid boundary. We use this model to examine the motion of a cell that is flowing at the interface between the cell-free layer and the central core region containing a high concentration of cells. The preceding discussion implies that a red blood cell traveling at this interface experiences a force directed away from the wall resulting from cell-wall interactions that is balanced by the lateral forces resulting from the cell-cell interactions generated by the shear flow in the suspending fluid. For this analysis, we represent the net

effect of cell-cell interactions (i.e., shear induced dispersion) by a prescribed lateral force f acting on the cell as shown in Figure 1 (b). We estimate the typical lateral force a cell would experience as a result of cell-cell interactions from previous observations of shear-induced dispersion. This estimate is used to predict the behavior of a red blood cell at the edge of the central core region of blood flowing in narrow tubes.

II. METHODS

A. Simulation of Red Blood Cells

A previously described two-dimensional (2D) model is used to represent the motion and deformation of the red blood cell [10, 11]. 2D models have been used in a number of previous theoretical studies of deformation and lateral migration of vesicles and red blood cells in channel flow [12–17]. Such models allow representation of the main fluid mechanical phenomena involved, e.g., proximity to boundaries, cell deformation, and cyclic "tank-treading" motion of the membrane around the cell interior.

A potential limitation of 2D models for red blood cells relates to the simulation of tank-treading motions. In a 2D model, the tank-treading motion requires only bending deformation of the membrane. However, a three-dimensional red blood cell experiences out-of-plane shear deformation during tank-treading, as bands of membrane around the cell are alternately lengthened and shortened (Figure 2 (a), (b)). This continuous deformation results in viscous energy dissipation in the membrane [18], and neglect of this effect leads to overestimation of tank-treading rates [19, 20].

The model used here is designed to account for this effect [11]. Red blood cells are represented in terms of their cross-sections in a plane through the center of the cell. The cell membrane is modeled as a set of straight, viscoelastic elements connected at nodes which act as elastic hinges representing the cell membrane's resistance to bending. This model also includes a central node which is connected to all external nodes by purely viscous elements as shown in Figure 2 (c). The fluid motion in the interior of the cell is not explicitly computed. The viscous internal elements are used to represent both the viscosity of the cell's interior and the cell membrane's viscous resistance to three-dimensional out-of-plane deformations.

In the approach used here, the equations of mechanical equilibrium are imposed exactly at each node. This approach was taken to minimize numerical errors that could affect the predicted lateral migration of cells, as could arise if the continuum equations of the membrane were represented in discrete form. A finite-element method is used to solve the equations governing the flow external to the cell, simultaneously with the equations of equilibrium at the nodes of the model cell. In previous work [11], this model was shown to give results for tank-treading frequency and elongation of a cell suspended in a viscous shear flow that agree closely with experimental observations.

The nodes and elements are numbered $j = 1, \ldots, N$ where N is the total number of external nodes. The external elements of the model cell have forces acting on them as a result of the fluid flow. Consequently, the longitudinal (tension) force $t_j(s)$, transverse (shear) force $q_j(s)$,

and bending moment $m_j(s)$ acting in the external element j are functions of distance s along the element from the node j to node $j + 1$, where $s \in [0, l_j]$ and l_j is the length of the external element j. The equations of mechanical equilibrium are:

$$\frac{dt_j}{ds} = -g_j \quad \frac{dq_j}{ds} = -f_j \quad \frac{dm_j}{ds} = q_j \quad (1)$$

where $f_j(s)$ and $g_j(s)$ are the normal and tangential components of the fluid loading. The average tension $\overline{t_j}$ in the jth external element is given by an elastic term proportional to its extension and a viscous term proportional to its rate of extension, according to a Kelvin-Voigt model. The tension T_j in the jth internal element is given by a purely viscous term. The bending moment at the jth external node is proportional to the difference of the orientations of the adjacent external elements.

The interior of a three-dimensional red blood cell is effectively incompressible, so that it deforms at constant volume, and thus the membrane deforms at nearly constant surface area. In two dimensions, the analogous properties are the perimeter and area in the model-cell plane. These properties are not kept constant, but are constrained to values that would represent the possible shapes of a three-dimensional cell with fixed surface area and volume. In the model, variations of perimeter are resisted by elastic control over element lengths, and variations of cell area A are resisted by assigning an interior pressure to the cell:

$$p_{int} = k_p(1 - A/A_{ref}) \quad (2)$$

where A_{ref} and k_p are constants.

With φ_j defined as the angle from reference of the internal element j and θ_j defined as the angle from reference of the external element j, the equilibrium equations for the x-component of the forces at node j are:

$$t_j(0)cos\theta_j - t_k(l_k)cos\theta_k - q_j(0)sin\theta_j + q_k(l_k)sin\theta_k + T_j cos\phi_j = 0 \quad (3)$$

where $k = j - 1$ ($k = N$ if $j = 1$).

In shear-induced dispersion, a cell experiences a spatially and temporally varying lateral force resulting from transient hydrodynamic interactions with other cells. In this analysis, we approximate this effect by applying a force directed towards the wall at each external node in the two-dimensional model cell. It is constant in time and acts equally on all nodes. This assumption neglects any cell deformations resulting from the non-uniform distribution of forces resulting from cell-cell interactions. The equilibrium equations for the y-component of forces at node j are:

$$t_j(0)sin\theta_j - t_k(l_k)sin\theta_k + q_j(0)cos\theta_j - q_k(l_k)cos\theta_k + T_j sin\phi_j = f \quad (4)$$

where f is the lateral force applied at each node and $k = j-1$ ($k = N$ if $j = 1$). The total force applied to the cell is then $Nf = F$. Equilibrium of forces at the central node results in:

$$\sum_{j=1}^{N} T_j cos\phi_j = \sum_{j=1}^{N} T_j sin\phi_j = 0 \quad (5)$$

B. Equations of Fluid Flow

The suspending medium is assumed to be an incompressible fluid with zero Reynolds number, so that the inertial effects of flow can be neglected and the governing equations are those of Stokes flow. The pressure and velocity components fields are expressed as $p(x, y)$ and $\mathbf{u}(x, y)$ where $\mathbf{u} = (u, \upsilon)$. The components of stress are:

$$\sigma_{xx} = 2\mu \frac{\partial u}{\partial x} - p \quad \sigma_{xy} = \mu \left(\frac{\partial u}{\partial y} + \frac{\partial v}{\partial x} \right) \quad \sigma_{yy} = 2\mu \frac{\partial v}{\partial y} - p \quad (6)$$

where μ is the fluid viscosity. The equations for equilibrium of stresses yield:

$$\frac{\partial \sigma_{xx}}{\partial x} + \frac{\partial \sigma_{xy}}{\partial y} = 0 \quad \frac{\partial \sigma_{xy}}{\partial x} + \frac{\partial \sigma_{yy}}{\partial y} = 0 \quad (7)$$

The divergence of the velocity field is given by:

$$e = \frac{\partial u}{\partial x} + \frac{\partial v}{\partial y} \quad (8)$$

with $e = 0$ for an incompressible fluid.

The fluid loadings on segment j are:

$$f_j = -p_{int} - \sigma_{xx} sin^2\theta_j + 2\sigma_{xy} sin\theta_j cos\theta_j - \sigma_{yy} cos^2\theta_j \quad (9)$$

$$g_j = (\sigma_{xx} - \sigma_{yy}) sin\theta_j cos\theta_j - \sigma_{xy} (cos^2\theta_j - sin^2\theta_j) \quad (10)$$

No-slip conditions for the cell's velocity are imposed along the membrane, so that the local fluid and cell velocities match. By combining equations 1–10, the equilibrium equations for a given configuration of the cell can be expressed as a linear system with the velocity and pressure fields in the fluid and the velocities of the nodes as unknowns. The resulting coupled system of equations is used to compute the cell's motion.

For this analysis, we wish to examine a single cell's interactions with a single boundary. Therefore, we consider the case in which the channel is relatively wide, so that the effects of the more distant wall are negligible, and the cell is suspended near the boundary of an effectively semi-infinite shear flow. The boundary conditions are taken to be $u(x, -w) = 0$ and $u(x, w) = 2\gamma w$ where $2w$ is the channel width and γ is the shear rate in the absence of a cell.

C. Computational Method

The system of coupled equations for the cell's motion along with the surrounding fluid is solved using a finite-element package (FlexPDE version 5.1.4, PDE Solutions Inc., Antioch, CA). Quadratic elements are used. Because of the structure of FlexPDE, the incompressibility condition, $e = 0$ cannot be specified, but instead the condition:

$$\nabla^2 p = K\epsilon \quad (11)$$

where K is a large value, approximately satisfies the condition. Generally, $N = 20$ nodes are used to represent the red blood cell.

At each time step, the red blood cell shape is placed in the fluid domain. The equations of Stokes flow are applied in the domain external to the cell. The fluid loadings on the external elements of the cell are computed in terms of the fluid flow and pressure fields, and are included in the equilibrium equations for forces acting at each node. In this way, the equations governing both the external fluid and the cell are explicitly coupled and are solved simultaneously using the FlexPDE package. The cell shapes are then updated using the computed nodal velocities and specified time step, using an explicit Euler scheme.

With regard to numerical error, the FlexPDE package automatically refines the domain's mesh until the solution errors are within a specified tolerance. Since an explicit scheme is used, a sufficiently small time step must be used. If the time step is too large, numerical instabilities are evident and the nodes of the cell oscillate. The time step is chosen so that these instabilities do not occur in any of the reported simulations and is taken to be either 0.25 or 0.5 ms.

D. Parameter Values and Initial Conditions

The procedures for setting the dimensions and material parameters of the cell were described previously [10, 11]. The initial condition for the cell shape is an ellipse with an aspect ratio of 2:1 and initial angle $\frac{\pi}{6}$ relative to the wall axis (Figure 3). The initial trajectory of the cell is sensitive to the initial condition, but the eventual type of motion generated under a given load is not sensitive to this assumption. Shear rates are varied between 100 s^{-1} and 600 s^{-1}, which is a relevant range of values for blood flow in microvessels [7]. Lateral forces are varied between $F = 0$ and $F = 6 \times 10^{-7}$ dyn where $F = Nf$ is the total applied lateral force.

The capillary number is defined as:

$$Ca = \frac{\mu r_0 \dot{\gamma}}{k_t} \quad (12)$$

where $\mu = 1$ cP is the viscosity of the suspending medium, $r_0 = 2.66$ μm is the reference radius of the cell, $\dot{\gamma}$ is the shear rate, and $k_t = 1.2 \times 10^{-5}$ N/m is the shear elastic modulus of the membrane. The capillary number varies between $Ca \approx 0.02$ and $Ca \approx 0.13$, depending on the shear rate.

E. Description of Particle Motion

In general, the system has $2(N + 1)$ degrees of freedom, representing the two-dimensional coordinates of N external nodes and the central node. In order to analyze particle dynamics, it is useful to define a smaller set of variables that describe the main features of the particle motion and shape. One key variable is the lateral position, described by the minimum distance between the cell and the wall. A second key variable is an angle θ representing the orientation of the long axis of the cell shape, similar to that defined by Keller and Skalak [21]. For a deformed cell lacking an axis of symmetry, this definition is ambiguous. Here, an inertia tensor is defined as [22]:

$$\mathbf{I}=\begin{pmatrix} I_{xx} & I_{xy} \\ I_{xy} & I_{yy} \end{pmatrix} \quad (13)$$

with

$$I_{xx}=\sum_{j=1}^{N} y_j^2 \quad I_{xy}=\sum_{j=1}^{N} -x_j y_j \quad I_{yy}=\sum_{j=1}^{N} x_j^2 \quad (14)$$

where (x_j, y_j) is the coordinate of the jth node. The particle orientation θ is then defined as the angle between the eigenvector of **I** with the smaller eigenvalue and the flow direction, resulting in an angle in the interval $[\frac{-\pi}{2}, \frac{\pi}{2}.$

The characteristic motions of the model red blood cell can be described in terms of these variables. Tumbling is defined by a continually decreasing θ, tank-treading is defined by a stable θ, and swinging is defined by fluctuations in θ. For a flexible particle, both swinging and tumbling motions involve fluctuations in the major and minor axes of the particle shape. In the case of a swinging cell, the resulting motion is also described as “vacillating-breathing” [23].

III. RESULTS

The predicted behaviors of the model red blood cell at three different levels of applied lateral force are illustrated in Figures 4 and 5. In the absence of a force, migration away from the wall is expected [9]. When a small force is applied, the cell executes a tumbling motion, as indicated by large variations in the minimum distance from the wall and complete cycles of the orientation angle θ. This is illustrated for the case $F = 4 \times 10^{-8}$ dyn, near the maximum force that permits tumbling. The oscillations in the distance from the wall are a result of the tumbling motion. Generally, the cell moves away from the wall when it has a positive orientation angle, and towards the wall when the orientation angle is negative. Similar behavior is observed in the absence of a lateral force (results not shown). When a large lateral force ($F = 1.6 \times 10^{-7}$ dyn) is applied, the cell rapidly approaches a stable position and shape, and executes a tank-treading motion. When an intermediate force is applied ($F = 6 \times 10^{-8}$ dyn), a transient swinging motion occurs, in which both the minimum distance from the wall and the orientation angle show decaying oscillations approaching stable values, associated with a tank-treading motion. Examples of the resulting cell shapes

in each case are shown in Figure 4. The time-dependent variation of the minimum distance from the wall and the orientation angle are shown in Figure 5 (a), (b).

Figure 5 (c) displays phase-plane type plots for the orientation angle and the minimum distance from the wall. For the corresponding problem with a rigid particle, these two variables would fully define the state of the system and the trajectory through each point in the phase plane would generally be unique. This property does not hold here, as a result of the multiple degrees of freedom associated with cell shape. When a small load is applied ($F = 4 \times 10^{-8}$ dyn), the successive trajectories associated with tumbling motions show variations resulting from shape changes. When $F = 3 \times 10^{-9}$ dyn, the minimum distance from the wall and the orientation angle show decaying uctuations and approach a fixed point. When $F = 8 \times 10^{-9}$ dyn, both variables rapidly approach a fixed point.

In Figure 6, the occurrence of tumbling, transient swinging, and tank-treading motions is shown in the parameter space defined by shear rate and total applied lateral force. For all shear rates considered, a transition from tumbling through transient swinging to tank-treading was found with increasing lateral force. With increasing shear rate, the lateral forces at which these transitions occurred increased.

IV. DISCUSSION

The simulations were carried out for a low suspending viscosity (1 cP) close to that of blood plasma. With this viscosity, an isolated red blood cell in an unbounded shear flow would tumble [21]. This behavior persists even if the initial position is very close to the wall in the absence of a lateral force. If the particle were rigid, it would execute a tumbling motion with periodic oscillations in the distance of the particle from the wall [24, 25]. A similar motion is predicted for the model red blood cell in the absence of a lateral force or when a small force is applied ($F = 4 \times 10^{-8}$ dyn, Figure 5). However, the motion of the model cell is more complex and non-periodic as a result of the defomation of the particle. Further increases in the lateral force lead to a stable tank-treading motion, possibly after a transient swinging motion ($F = 6 \times 10^{-8}$ or 1.6×10^{-7} dyn, Figure 5).

The effect of imposing a lateral force can be interpreted as follows. Proximity to a solid boundary tends to inhibit tumbling motion of an elongated particle. In the absence of a lateral force, the cell moves sufficiently far from the wall such that tumbling can occur. Application of a sufficiently large lateral force keeps the cell close to the wall, such that tumbling is inhibited. For any given shear rate, continuous tumbling is prevented and stable tank-treading eventually occurs when the lateral force exceeds a threshold value. The initial transient period of swinging motion decreases with increases in lateral force.

In this system, inertial forces are negligible, and the applied lateral force must at all times be balanced by a hydrodynamic “lift” force generated by the cell’s motion. Such a force could, for example, be generated by fluid drag if a particle moves towards the wall. However, this does not apply to a stable tank-treading motion at a fixed distance from the wall. In that case, the lift must result from the asymmetry of the cell’s shape or orientation. As known from classic lubrication theory for a slider bearing [26], inclination away from the wall in

the direction of motion generates lift. Moreover, Olla [27] showed that for a tank-treading ellipsoid, the generation of lift was dependent on the fixed, positive orientation of the cell. As shown in Figure 5 (b) ($F = 6 \times 10^{-8}$ or 1.6×10^{-7} dyn), tank-treading motions exhibit a slightly positive orientation angle. The cell's fixed, positive orientation relative to the boundary is evidently a key factor for the generation of lift.

In tumbling motions, cells experience all possible orientation angles and yet are able to generate lift. In the tumbling simulations presented here, the orientation angle remains at small, positive values through most of the cycle ($F = 4 \times 10^{-8}$ dyn, Figure 5 (b)), and the positive orientation angle is likely responsible for the generation of lift. This argument is supported by phase-plane plots (Figure 5 (c)), where migration away from the wall is generally associated with a positive orientation angle, and more time spent with a positive orientation angle would lead to migration away from the wall. This behavior can be further examined using the phase-plane plot for tumbling ($F = 4 \times 10^{-8}$ dyn, Figure 5 (c)). For a given magnitude of the orientation angle (e.g., $\theta = \pm \frac{\pi}{4}$), the typical distance from the wall is smaller for $\theta > 0$ than $\theta < 0$. The increase in distance from the wall occurs during the period of small, positive orientation angle (indicated by the shaded region). This effect is a consequence of particle deformability and would not be found for an elongated rigid particle [24].

Grandchamp et al. [9] determined a scaling law for the lift of tumbling red blood cells. However, the cells' distance from the wall in the Grandchamp et al. [9] results are significantly larger than those considered here, and the results presented here consider the effects of a lateral force. Thus, the results from Grandchamp et al. [9] are not directly comparable.

The applied lateral force is introduced in the present model to represent the effects of cell-cell interactions on a cell traveling at the edge of the cell-free layer. These effects can be viewed as an example of the phenomenon of shear-induced dispersion, in which particle-particle interactions in shear flow on average lead to a drift of particles down their concentration gradient [4, 9]. We use a previously developed theory of shear-induced dispersion to estimate the resulting lateral force. In their analysis of the factors determining the width of the cell-free layer, Pranay et al. [8] described the local flux of cells j_y normal to the wall as:

$$j_y = u_{mig}\phi - D_g \frac{\partial \phi}{\partial y} \quad (15)$$

where u_{mig} is the wall-induced migrational velocity of the cell, φ is the volume fraction of the cells. Here, we use their analysis to estimate the typical force F_{SID} acting on a cell as a result of shear-induced diffusion. The gradient diffusivity of a dilute suspension of cells D_g is estimated as [28, 29]:

$$D_g = \gamma \phi a^2 f_s \quad (16)$$

where a is the radius of the cells and f_s is a coefficient which depends on the deformability and shape of the cells. This assumes that D_g is dominated by pairwise interactions and neglects the effect of higher order interactions. In an experimental study of the shear-induced dispersion of red blood cells, Grandchamp et al. [9] estimated $f_s \approx 1.7$.

We approximate the relationship between velocity and force by Stokes law for the drag on a sphere. The force induced by shear-induced dispersion F_{SID} can then be written as:

$$F_{SID}=6\pi\mu a D_g \frac{\partial \phi}{\partial y}=6\pi\mu\gamma\phi a^3 f_s \frac{\partial \phi}{\partial y} \quad (17)$$

If we denote the concentration of the red blood cell core as φ_{core}, then we can approximate $\varphi \approx \varphi_{core}$ and $\frac{\partial \phi}{\partial y} \approx \frac{\phi_{core}}{a}$ since the volume fraction drops to zero over a distance comparable to the radius of the cell [30]. With typical values $\mu = 1$ cP and $a = 3.6$ μm, the estimated loading is:

$$F_{SID}=4.15\phi^2\gamma \times 10^{-8}\text{dyns} \quad (18)$$

The results shown in Figure 6 can be used to infer the likely motion of a cell at the interface of the cell-free layer and the red blood cell core. This reasoning indicates that unless the hematocrit is very low, the cells are stabilized at the edge of the layer and tank-tread for the shear rates studied. Furthermore, as F_{SID} has a quadratic dependence on φ, when the hematocrit is decreased the decrease in F_{SID} may result in tumbling. The hematocrit at which this transition occurs is dependent on the shear rate and occurs at $\varphi \approx 0.06$. These results are consistent with experimental observations showing tumbling at dilute concentrations [3, 9] and tank-treading at higher concentrations [31].

The estimate of F_{SID} relies on a formulation of the theory of shear-induced dispersion assuming a dilute suspension. As the concentration of cells is increased, higher order interactions influence shear-induced dispersion. Grandchamp et al. [9] determined the coefficient at higher concentrations, demonstrating that interactions resulting from three-body interactions add to the overall dispersion of the suspension. This implies that the hematocrit determined above at which the transition from tumbling to tank-treading occurs should be considered a lower bound, and the transition would likely occur at a lower hematocrit if effects of higher-order interactions are considered.

In summary, our simulations of red blood cell motion in shear flow have introduced a new mechanism for the stabilization of cell orientation, leading to tank-treading. This mechanism depends on the presence of a lateral force acting on the cell and driving it towards a solid boundary. For a small lateral force, tumbling still occurs, and a corresponding lift is generated as a result of the tendency of the cell to remain at a small, positive orientation during its tumbling cycle. With a larger lateral force, the cell is driven closer to the wall, such that tumbling is inhibited and the stable tank-treading motion occurs with a fixed, positive orientation. Estimates of the lateral force on a cell at the edge of the cell-rich core in tube flow lead to the prediction of tank-treading at physiological hematocrits and tumbling

at lower hematocrits. These predictions are based on several simplifying assumptions including: the use of a two-dimensional model, the representation of cell-cell interactions as a constant force, and the estimation of the force using a theory that considers only pairwise interactions. The physical insights and predictions resulting from this work can be tested by comparisons with experimental observations or corresponding detailed multi-cell simulations.

ACKNOWLEDGMENTS

This work was supported by the National Institute of Health (NIH) Grant No. HL034555.

References

1. Fahraeus R, Lindqvist T. Am. J. Physiol. 1931; 96:562.
2. Secomb TW. Symp. Soc. Exp. Biol. 1995; 49:305. [PubMed: 8571232]
3. Goldsmith HL. Fed. Proc. 1971; 30:1578. [PubMed: 5119364]
4. Leighton D, Acrivos A. J. Fluid Mech. 1987; 181:415.
5. Secomb, TW. Modeling and Simulation of Capsules and Biological Cells. Pozrikids, C., editor. Boca Raton, Florida: Chapman & Hall/CRC; 2003. p. 163-196.
6. Fedosov DA, Caswell B, Popel AS, Karniadakis GE. Microcirc. 2010; 17:615.
7. Pries AR, Neuhaus D, Gaehtgens P. Am. J. Physiol. 1992; 263:H1770. [PubMed: 1481902]
8. Pranay P, Henríquez-Rivera RG, Graham MD. Phys. Fluids. 2012; 24:061902.
9. Grandchamp X, Coupier G, Srivastav A, Minetti C, Podgorski T. Phys. Rev. Lett. 2013; 110:108101. [PubMed: 23521300]
10. Barber JO, Alberding JP, Restrepo JM, Secomb TW. Ann. Biomed. Eng. 2008; 36:1690. [PubMed: 18686035]
11. Secomb TW, Styp-Rekowska B, Pries AR. Ann. Biomed. Eng. 2007; 35:755. [PubMed: 17380392]
12. Beaucourt J, Biben T, Misbah C. Europhys. Lett. 2004; 67:676.
13. Cantat I, Misbah C. Phys. Rev. Lett. 1999; 83:880.
14. Freund JB. Phys. Fluids. 2007; 19:023301.
15. Kaoui B, Ristow GH, Cantat I, Misbah C, Zimmermann W. Phys. Rev. E. 2008; 77:021903.
16. Kaoui B, Biros G, Misbah C. Phys. Rev. Lett. 2009; 103:188101. [PubMed: 19905834]
17. Secomb TW, Skalak R. Microvasc. Res. 1982; 24:194. [PubMed: 7176938]
18. Fischer TM. Biophys. J. 1980; 32:863. [PubMed: 7260306]
19. Hsu R, Secomb TW. J. Biomech. Eng. 1989; 111:147. [PubMed: 2733409]
20. Fedosov DA, Caswell B, Karniadakis GE. Bio-phys. J. 2010; 98:2215.
21. Keller SR, Skalak R. J. Fluid Mech. 1982; 120:27.
22. Freund JB, Orescanin MM. J. Fluid Mech. 2011; 671:466.
23. Misbah C. Phys. Rev. Lett. 2006; 96:028104. [PubMed: 16486649]
24. Bretherton FP. J. Fluid Mech. 1962; 14:284.
25. Hsu R, Ganatos P. J. Fluid Mech. 1994; 268:267.
26. Cameron, A. The Principles of Lubrication. New York: Wiley; 1966.
27. Olla P. J. Phys. (Paris). 1997; 7:1533.
28. Da Cunha FR, Hinch EJ. J. Fluid Mech. 1996; 309:211.
29. Loewenberg M, Hinch EJ. J. Fluid Mech. 1997; 338:299.
30. Aarts PA, Van Den Broek SA, Prins GW, Kuiken GD, Sixma JJ, Heethaar RM. Arter., Thromb., Vasc. Biol. 1988; 8:819.
31. Fischer TM. Blood Cells. 1978; 4:453.

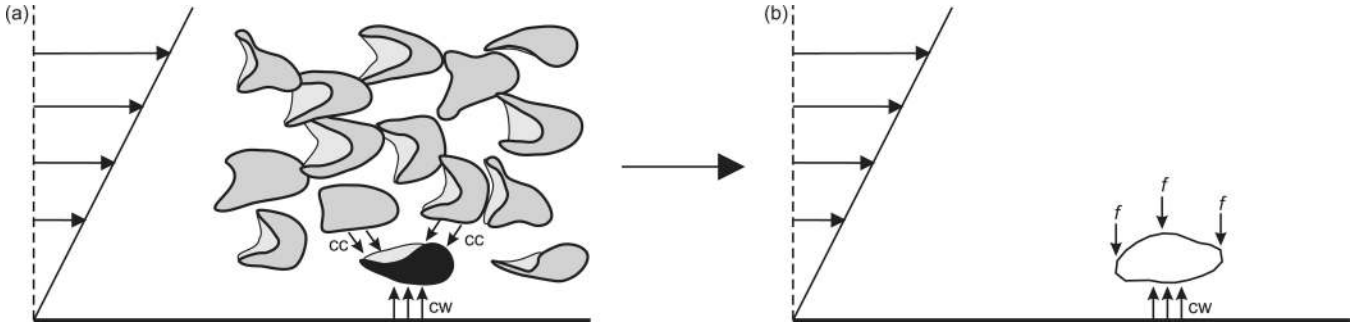

Figure 1.

(a) Schematic diagram of the force balance between cell-cell (cc) and cell-wall (cw) interactions. (b) Two-dimensional diagram of system analyzed here, in which an applied lateral force *f* is counteracted by cw interactions.

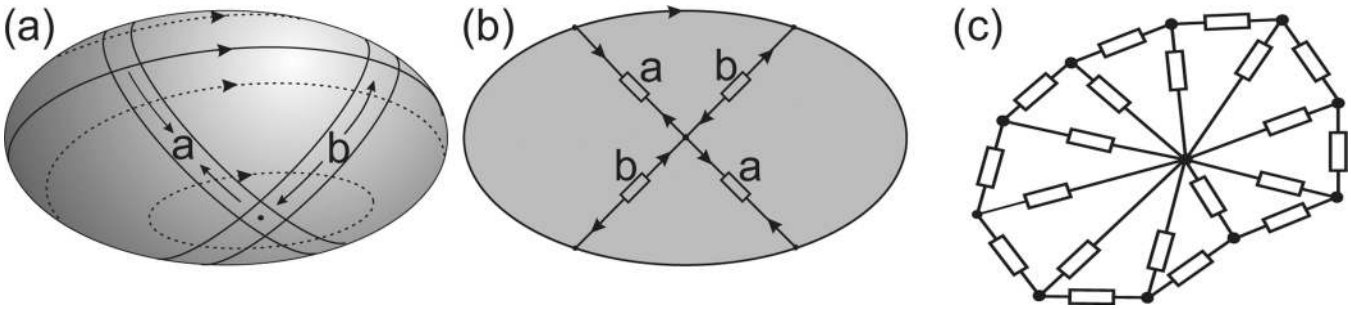

Figure 2.

(a) Example of a tank-treading three-dimensional ellipse, showing out-of-plane membrane deformation. Two bands of membrane around the cell are labeled a and b. At this point in the motion, band a is shortening and band b is lengthening. (b) Configuration of the two-dimensional model with interior elements labeled to correspond to the two bands of membrane shown in (a). (c) Two-dimensional model for the red blood cell. Rectangles represent viscous or viscoelastic elements.

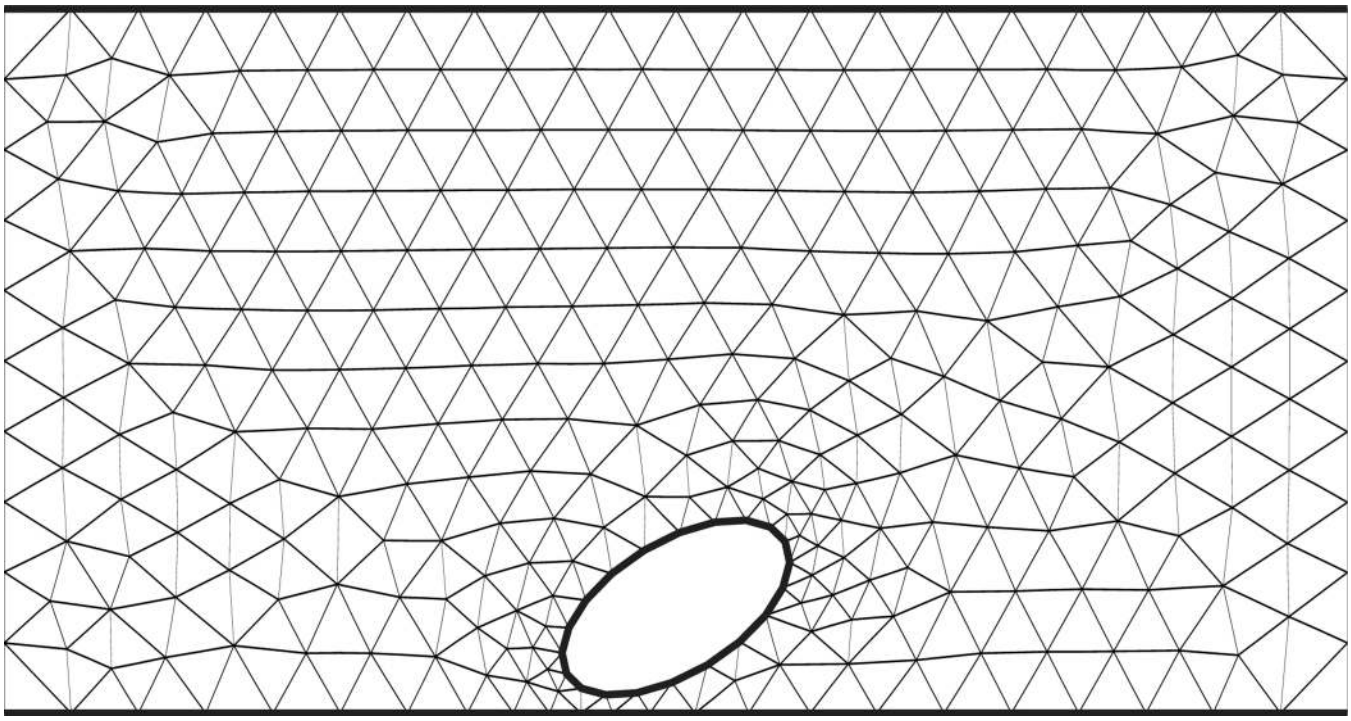

Figure 3.
Sample computational domain shown with generated mesh.

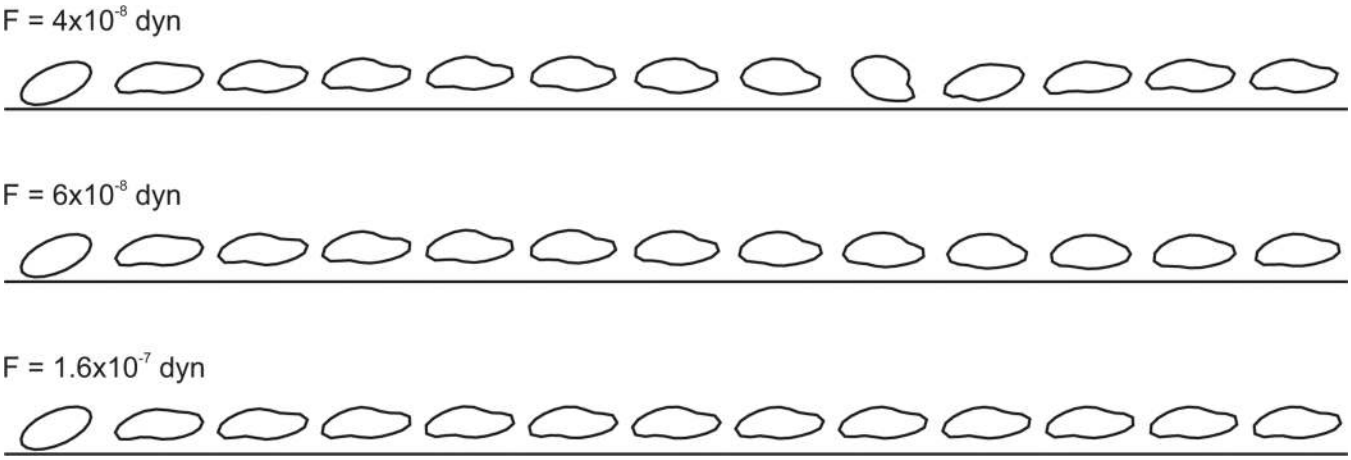

Figure 4.

Sample cell shapes with a shear rate of $\gamma = 400\ s^{-1}$ for $F = 4 \times 10^{-8}$, 6×10^{-8}, 1.6×10^{-7} dyn taken at equally spaced time intervals between $\gamma t = 0$ and $\gamma t = 96$

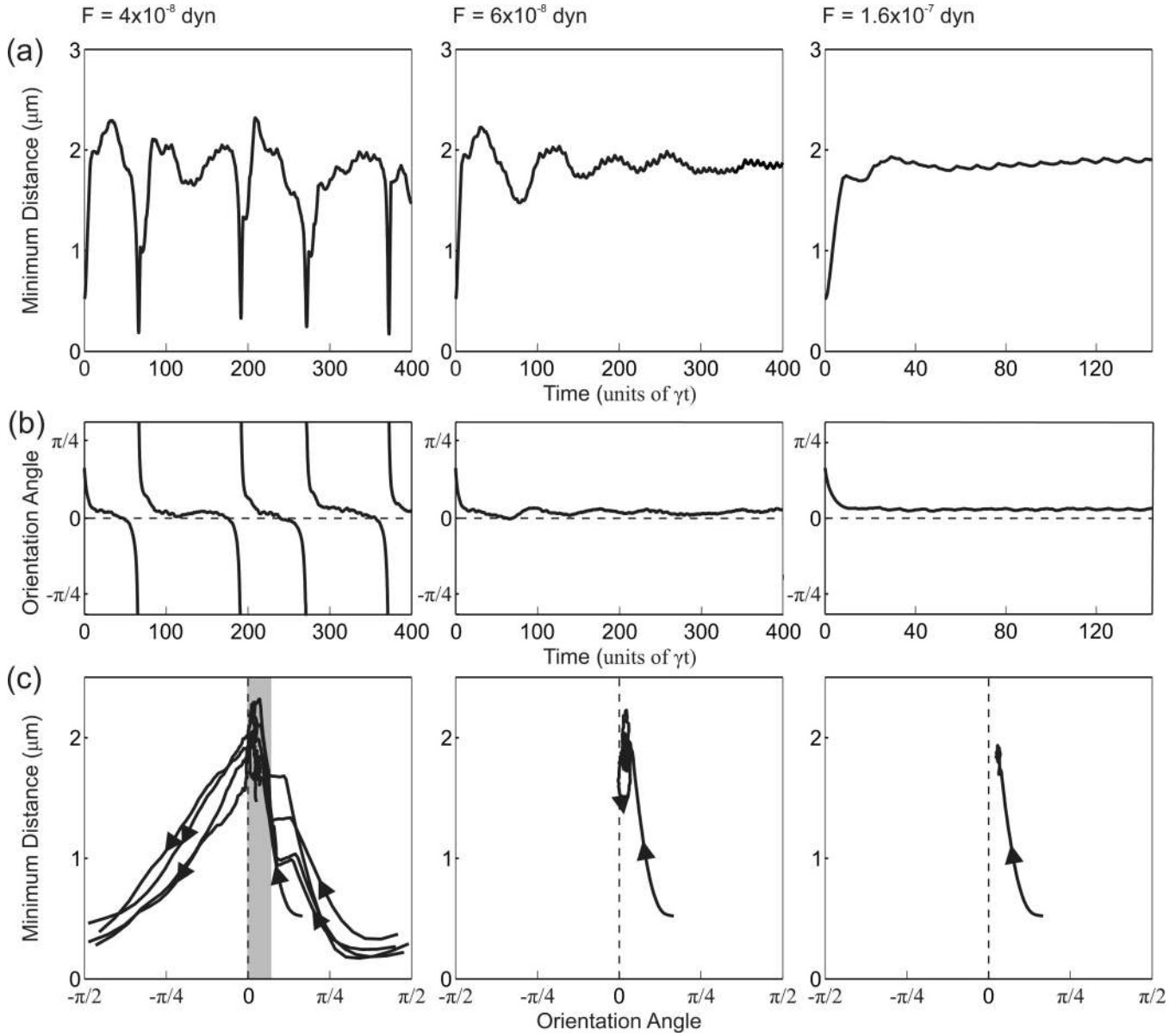

Figure 5.

Predicted behaviors for $\gamma = 400\ s^{-1}$ with $F = 4 \times 10^{-8}$, 6×10^{-8}, 1.6×10^{-7} dyn. (a) Time variation of minimum distance from the wall. (b) Time variation of orientation angle. Dashed lines indicate $\theta = 0$. (c) Phase plots of orientation angle against minimum distance from the wall. Shaded region contains parts of tumbling trajectories in which cells show a small, positive orientation angle and migrate away from the wall.

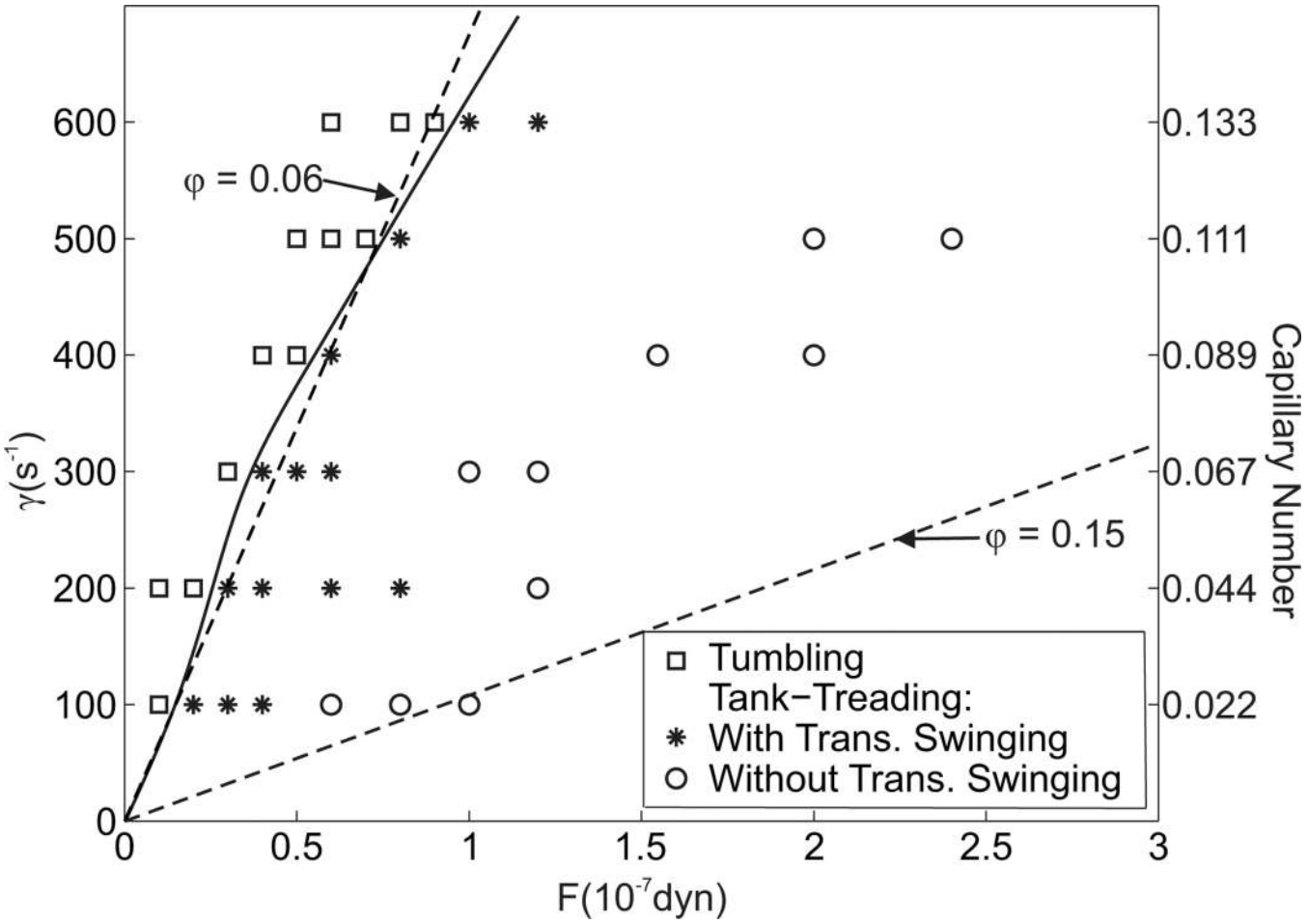

Figure 6.

Dependence of cell motion on lateral force and shear rate. Total lateral force is indicated as $F = Nf$ where N is the total number of external nodes. Dashed lines indicate estimates for F_{SID} with $\varphi = 0.06$ and $\varphi = 0.15$ based on Equation 18, and the solid curve indicates the transition from tumbling to tank-treading.